Transactions **of the SMiRT 27**
Yokohama, Japan, March 3-8, 2024
Division III

INTEGRITY ASSESSMENT INTERNALS OF PWR

Peter Baas[1], Marieke Hannink[2]

[1] Ing, NRG, Petten, The Netherlands (p.baas@nrg.eu)
[2] Dr.ir, NRG, Petten, The Netherlands

ABSTRACT

Stress Corrosion Cracking (SCC) is considered an important time dependent damage mechanism of the Reactor Pressure Vessel (RPV) internals for long term operation of Pressurized Water Reactors (PWR). This mechanism affects the bolts connecting the formers and baffles. An evaluation of stresses in the baffle and barrel bolts during different operational scenarios is carried out using thermo-mechanical finite element analyses.

The heat deposition and neutron fluence data for normal operation are obtained by reactor physics calculations. Effective heat transfer coefficients (HTC) are calculated by computational fluid dynamics (CFD). The following steps are performed for this work:

- Effective HTC and coolant temperatures as well as nominal heat deposition values are scaled to obtain a temperature distribution of the RPV internals during a transient startup – normal operation – SCRAM cycle.
- Irradiation creep and swelling analyses are conducted for a time span of 60 years taking into account a temperature distribution for normal operation.
- Thermo-mechanical SCRAM analyses are conducted with initial conditions taken at different moments in time from the creep and swelling analyses (different swelling states).
- Bolt stresses are evaluated and assessed for possible fatigue taking into account the different stress states.

The TMA models are developed using ANSYS Mechanical APDL (Ansys®, 2020R2), The RPV internal geometry created is based on a PWR design. 1/8th of the RPV internal geometry is considered for the CFD and FEA, taking advantage of symmetry to reduce calculation time.

INTRODUCTION

Stress Corrosion Cracking (SCC) is one of the most important time dependent, and therefore Long Term Operation (LTO) related, damage mechanisms of the reactor pressure vessel (RPV) internals. In some pressurized water reactors cracks have been found in the baffle to former bolts and core barrel to former bolts. Currently, no accurate methods are available to predict this kind of failure. Therefore, SCC of these bolts is internationally an important field of attention. Due to LTO and the associated increasing doses for the internals, the importance of this topic will increase in the future.

NRG aims to enhance modeling capabilities by integrating neutronics, Computational Fluid Dynamics (CFD), and Finite Element Analysis (FEA), incorporating advanced models for irradiation-assisted creep, swelling, and plasticity. The study involves an assessment of bolt stresses over a 60-year operational period using thermo-mechanical FEA, considering thermal, mechanical, and irradiation loads. Irradiation hardening and swelling models from Chopra (2010) and the irradiation-assisted creep model from Mitsubishi Heavy Industries (MHI) and Japan Nuclear Energy Safety (JNES) per Takakura et al. (2010) are utilized, providing the foundation for this analysis.

MODELLING APPROACH

The approach to assess the temperatures and stresses occurring throughout the RPV internals is separated in distinct analyses.

First, pre-existing thermal loads of the RPV internals during normal operation are loaded into ANSYS, these loads, derived from associated CFD and Neutronics (MCNP) analyses, are then scaled over time to simulate a startup – normal operation – SCRAM cycle. Subsequently, a transient thermal analysis of the complete cycle is performed.

The static structural analysis required the implementation of constitutional models for irradiation swelling and creep, as well as irradiation based material hardening. Implementation of these models is accomplished through Ansys User Programmable Features (UPF). The functionality of the implementation was verified by means of cubic (single) element models, comparing output to preexisting research data.

For the static structural analyses, a number of temperature distributions are transferred from the thermal transients analysis. Namely for the nominal operational condition and three from the SCRAM condition (at T+0.5, T+1.0 and T+10 s). These different temperature distributions are cyclically applied during the multi-step structural analysis.

Besides the thermal field, a neutron flux field is applied during the nominal operational condition of each cycle. This flux is henceforth referenced by the UPF subroutines userswstrain, usercreep and userfld to include irradiation induced swelling, creep and material hardening respectively.

RPV INTERNALS MODEL

The finite element model of the baffle-former-bolt and core barrel-former-bolt assembly is shown in Figure 1. The baffles, formers and core barrel are made of 1.4550 (i.e. AISI 347) while the bolts are made of 1.4571 (i.e. AISI 316Ti). Part of the mesh is unselected to give a clear view of the contact elements in between the different components, all of which are considered to transfer heat perfectly between the different components during the thermal analysis and, except for the bonded contact pairs simulating the threaded sections, exhibit frictional behavior (with a coefficient of 0.2) throughout the multiple structural analysis steps.

To expedite calculations, we opted for a relatively coarse mesh. For instance, the M16 baffle-former bolts in the top and bottom formers consist of 616 elements each, the M12 baffle-former bolts in the middle 5 formers have 300 elements each, and the M12 barrel bolts consist of 330 elements each. The entire set of bolts, comprising M16 and M12 types, totals 45,565 elements

The complete model consists of 881,011 nodes and 163,602 quadratic solid elements including the bolts. For the thermal analysis, the total number of elements is 311,990 including the SOLID279 elements and the multiple TARGE170 and CONTA174 elements facilitating thermal conductivity between the different components.

For the mechanical analysis, the solid element type is changed to SOLID186, the total number of elements is reduced to 298,629 since the contact elements used for implied water conductivity in the void between the bolt stems and their surrounding former material are not required. The remaining contacts are modified to exhibit mechanical contact.

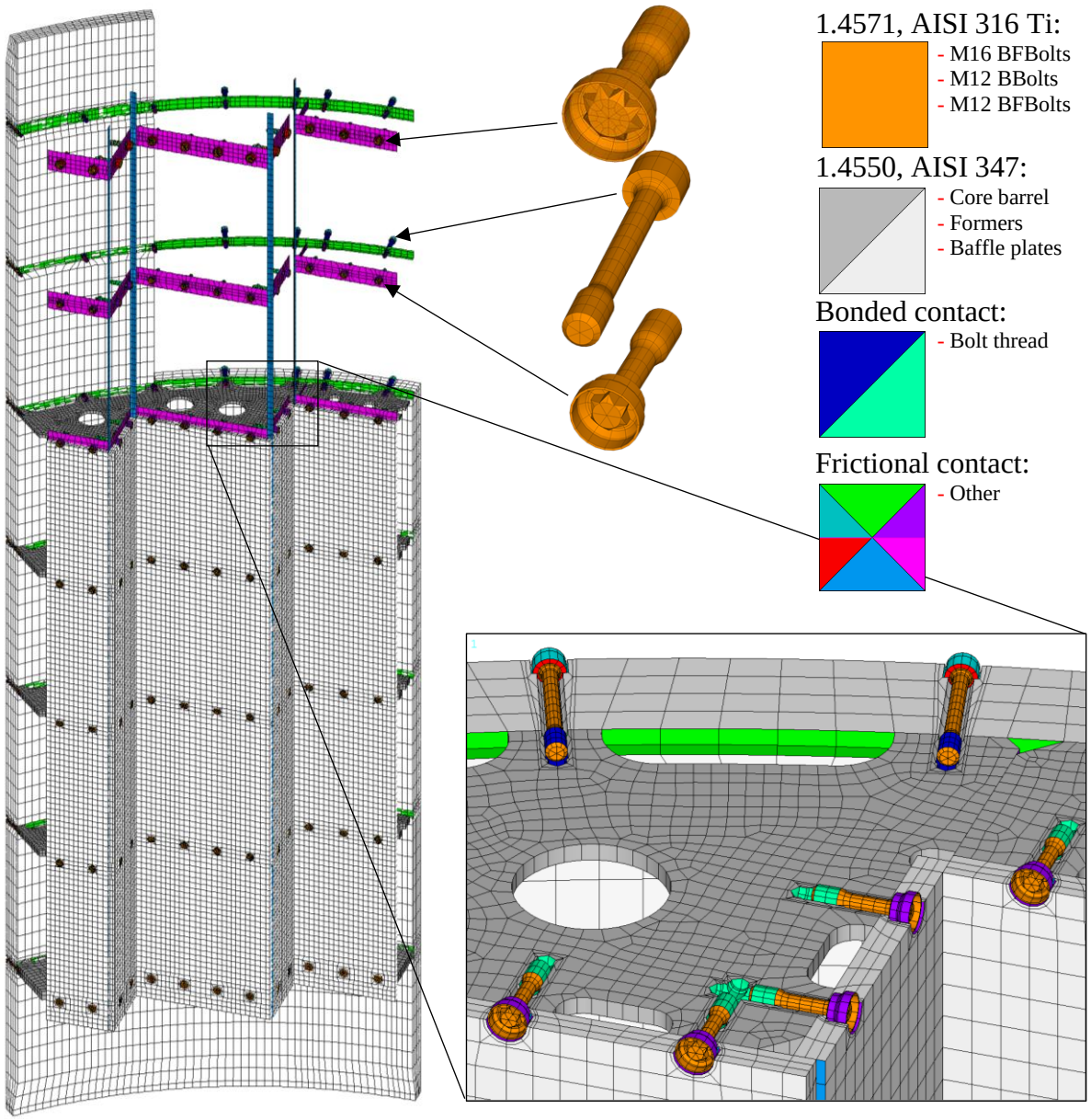

Figure 1. 1/8th RPV model, mesh, contact sets and material designation

The basic properties employed for the two materials are shown in Table 1. These properties were taken from previous work by Matteoli (2014), the original reference being DIN 17440 (1985). Other properties, related to irradiation hardening and swelling, substitute AISI304 for AISI347, owing to the fact that properties for the latter material could not be readily sourced.

Table 1: Material properties as implemented in the model.

T [°C]	ρ [kg/m^3]	C_p [J/kg·K]	k [W/m·K]	E [MPa]	ν [-]	α_{mean} [K^{-1}]	
						AISI347	*AISI316Ti*
20	7930	470	15	200000	0.3	1.60E-05	1.65E-05
100		470	16	194000		1.60E-05	1.65E-05
200		490	17	186000		1.70E-05	1.75E-05
300		500	19	179000		1.70E-05	1.75E-05
400		520	20	172000	0.3	1.80E-05	1.85E-05

IRRADIATION HARDENING

A multilinear isotropic hardening (MISO) model was used to implement instantaneous plastic deformation effects.

Equation 1 according to Chopra (2010) is used to calculate yield stress, ultimate stress and ultimate strain. Here, F refers to neutron dose [dpa] while the values for parameters A_0, A_1 and d_0 are listed in Table 2 and Table 3 for the materials AISI316Ti (cold worked) and AISI304 (annealed) respectively.

$$\text{Property} = A_0 + A_1\left(1 - \exp(-F/d_0)\right) \tag{1}$$

Table 2: Material property parameters for AISI316Ti

Property	Units	A_0	A_1	d_0
0.2% yield strength (YS)	MPa	500	470	3
Ultimate tensile strength (UTS)	MPa	650	330	3
Uniform elongation (e_u)	%	10	-9.7	2
Total elongation (e_t)	%	18	-11	5

Table 3: Material property parameters for AISI304

Property	Units	A_0	A_1	d_0
0.2% yield strength (YS)	MPa	200	600	3
Ultimate tensile strength (UTS)	MPa	450	350	3
Uniform elongation (e_u)	%	40	-39.5	1
Total elongation (e_t)	%	45	-37	2.5

The material properties are updated during the analysis by means of a user-defined field variable (TBFIELD,UF01), the field variable is updated every sub step by means of the subroutine userfld.F. The subroutine copies the current dpa state variable to the field variable at the beginning of each substep. After an accumulated dose of 27 dpa, the properties are assumed constant.

IRRADIATION SWELLING

Swelling equations according to Chopra (2010) have been implemented through the userswstrain subroutine. Two distinct equations are incorporated into the subroutine. The swelling rate SR (%/dpa) is expressed in terms of the temperature T (K), neutron dose F (dpa), and dose rate *Drate* (dpa/s). The swelling rate for annealed AISI 304 and cold worked AISI 316 are given by Equations 2 and 3 respectively.

$$\text{SR}_{\text{SA304}} = 2 \cdot \text{F} \cdot \left(\frac{Drate}{\text{1E-7}}\right)^{-0.731} \cdot \exp\left(22.106 - \frac{18558}{\text{T}}\right) \tag{2}$$

$$\text{SR}_{\text{CW316}} = 0.9 \cdot \left[10 + 2 \cdot \text{F} \cdot \left(1 - \exp(-0.01 \cdot F)\right)\right] \left(\frac{Drate}{\text{1E-7}}\right)^{-0.731} \cdot \exp\left(22.106 - \frac{18558}{\text{T}}\right) \tag{3}$$

The subroutine uses the material dependent swelling rate SR to calculate the swelling strain increment according to Equation 4. Where dF is the neutron dose increment (dpa) and σ is the equivalent von mises stress (Pa), making the swelling strain stress state dependent.

$$\text{dsweq} = \left(\left(\frac{SR}{100} \cdot \text{dF} \cdot \left(1 + 0.005 \cdot \frac{\sigma}{\text{1E-6}}\right)\right) + 1\right)^{\frac{1}{3}} - 1 \tag{4}$$

To verify the implementation of the swelling strain, a cubic element (1 m^3) model was used to compare its output with the existing plot from Chopra (2010) shown in Figure 2. Note that while the verification charts conform to the original underlying charts, the steeper 304 SS curve slightly deviates.

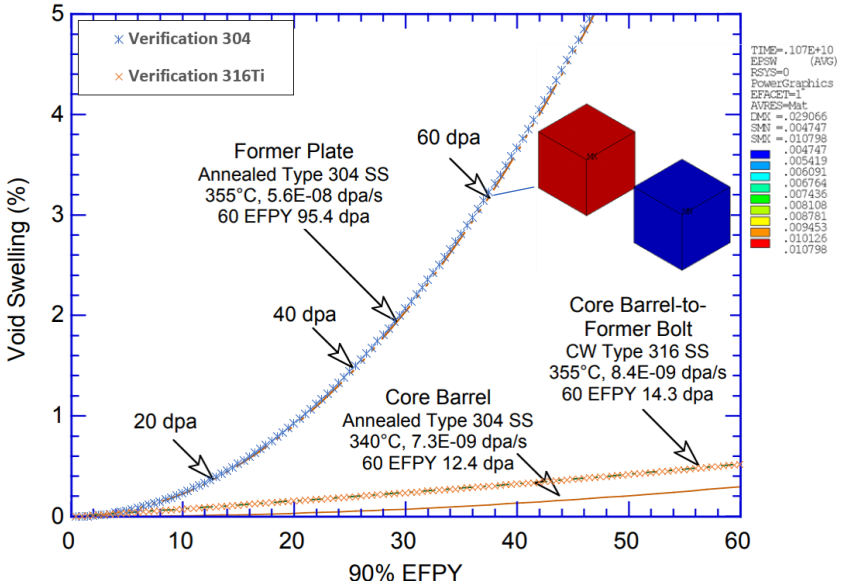

Figure 2. Swelling model implementation verification.

IRRADIATION CREEP

To account for irradiation creep, the equation according to Takakura et al. (2010) has been utilized. See Equation 5 for the original form.

$$\varepsilon_{cr} = A \cdot \sigma \cdot [1 - \exp(-A' \cdot F)] + B_0 \cdot \sigma \cdot (1 + B_1 \cdot \sigma^3) \cdot F \tag{5}$$

Where ε_{cr} is the creep strain (-), σ is the equivalent effective stress (MPa) and F is the neutron dose (dpa). The coefficients A, A', B_0 and B_1 are given in Table 4. Both the original values from Takakura et al. (2010) and the adjusted values utilized in this analysis are provided. The determination process for these modified coefficients is explained later in this chapter.

Table 4: Irradiation creep coefficients

	Original	Modified
A	7.33E-07	5.50E-06
A'	4.3	17.2
B_0	9.75E-07	3.90E-06
B_1	3.28E-09	1.64E-06

The following Equations 6 and 7 are employed in the Ansys usercreep subroutine.

$$\text{delcr} = \left\{A \cdot A' \cdot \exp(-A' \cdot F) + B_0 \cdot \left(1 + B_1 \cdot \left(\frac{\sigma}{1E6}\right)^3\right)\right\} \cdot \frac{\sigma}{1E6} \cdot dF \tag{6}$$

$$\text{dcrda}(1) = \text{delcr}/\sigma + 3 \cdot B_0 \cdot B_1 \cdot \sigma^3 \cdot \left(\frac{1}{1E6}\right)^4 \cdot dF \tag{7}$$

Where delcr is the creep increment (m/m), F is the neutron dose (dpa), σ is the equivalent effective stress (Pa) and dF is the neutron dose increment (dpa). The derivitive of incremental creep strain to effective stress, dcrda(1), is required for solver convergence.

The implementation of the creep model was verified by application of a fixed displacement (tensile) to a cubic element (1 m^3) model, shown in Figure 3. The displacement was chosen such that the initial stress was 100 MPa, a flux load was then applied to the elements, accumulating to a dose of 3 dpa over the load step. As the dose increases, the stress is reduced while the displacement remains constant.

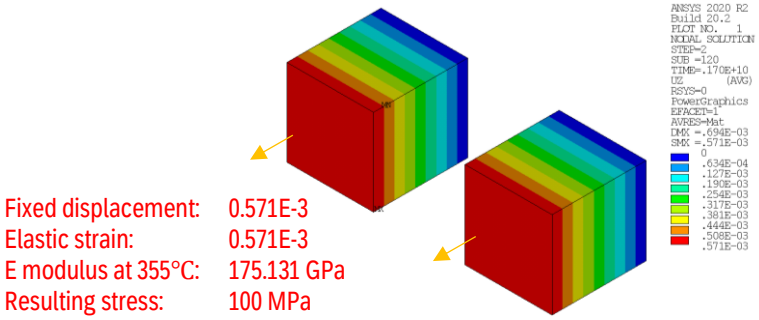

Figure 3. Creep model stress relaxation simulation.

The stress as function of dose was then plotted and overlaid on an existing graph from Chopra (2010) as shown in Figure 4. It can be noted that with the original coefficients for A, A', B_0 and B_1, the stress relaxation is mild compared to most datapoints shown in the graph. After iteratively modifying the coefficients, the results from the cubic element strain relaxation simulation display behavior comparable to the "trend line for screening irradiation-induced stress relaxation".

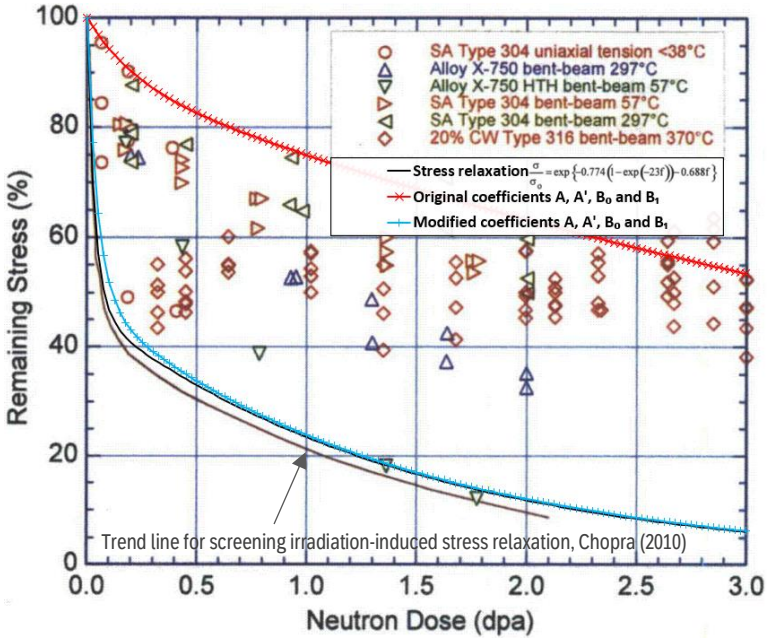

Figure 4. Creep model implementation verification and comparison.

Please note that the fitting of the implemented function from Takakura et al. (2010), involving the modification of coefficients, was carried out at an initial stress of 100 MPa. The response of the implementation has not yet been tested under various initial stress states. Notice also, that the stress relaxation formula provided by Chopra (2010), of which a curve is plotted and overlaid on the graph, does not match the trend line for screening. This was not investigated further currently.

Both the original and modified coefficients are utilized in separate structural analyses of the RPV internals to gauge the importance of these properties for (cyclic) stress calculations.

THERMAL TRANSIENT ANALYSIS

The thermal transient analysis comprises multiple load steps, though focus is directed solely towards the nominal condition and consecutive SCRAM distributions, which are of interest for the subsequent mechanical analysis. Figure 5 visually depicts the thermal loads applied to the model during the nominal operational condition, encompassing volumetric heating (W/m³) and convective heat transfer, where the bulk temperature (K) and heat transfer coefficient (W/m²/K) are specified.

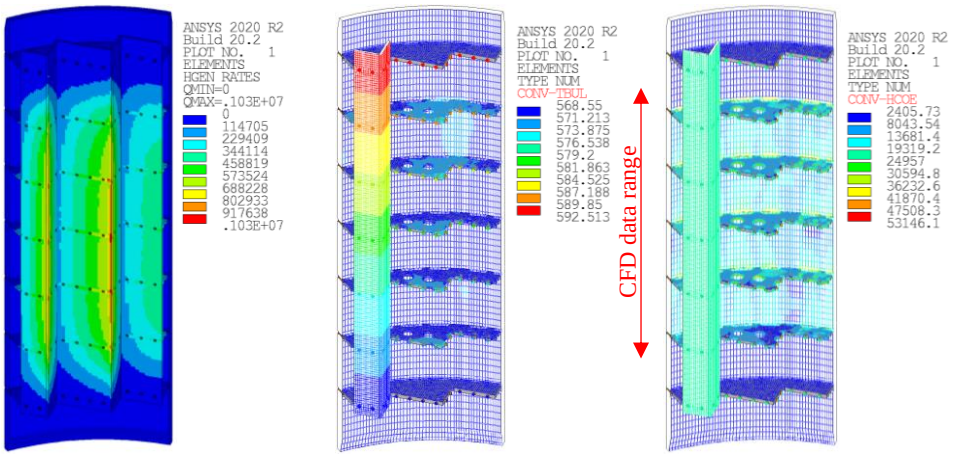

Figure 5. Heating [W/m³] (left), bulk temperature [K] and heat transfer coefficient [W/m²/K]

Volumetric heating was determined by multiplying nuclear heating (W/g) from MCNP with material density. The convection boundary relied on CFD analysis, which was limited to bypass surfaces surrounding the middle 5 formers as pointed out by the range arrow. Top and bottom former conditions were manually input, assuming inlet/outlet temperatures of 295.4 and 298.0 °C, with a constant heat transfer coefficient of 4000 W/m²/K. A uniform bulk temperature of 295.4 °C was assumed outside the barrel. On the core-facing side of the baffle plates, the bulk temperature was presumed to increase linearly from 295.4 to 319.4 °C. For both the outside of the barrel and the core-facing side of the baffle plates, a constant HTC of 22500 W/m²/K was assumed. During a SCRAM condition, volumetric heating dropped from 100% to 6.7%, and convection conditions were altered, inducing thermal gradients.

Transient temperature distributions were assessed using TGSUM plots, revealing increased thermal gradients during SCRAM. Figure 6 compares nominal and SCRAM conditions for bolts, showing doubled thermal gradients in SCRAM. Though the actual thermal gradient is expected to be smaller due to latent heat and nuclear heating affecting the bulk temperature of the water, we went forward with this data to gauge the maximum possible effect of this “thermal shock”.

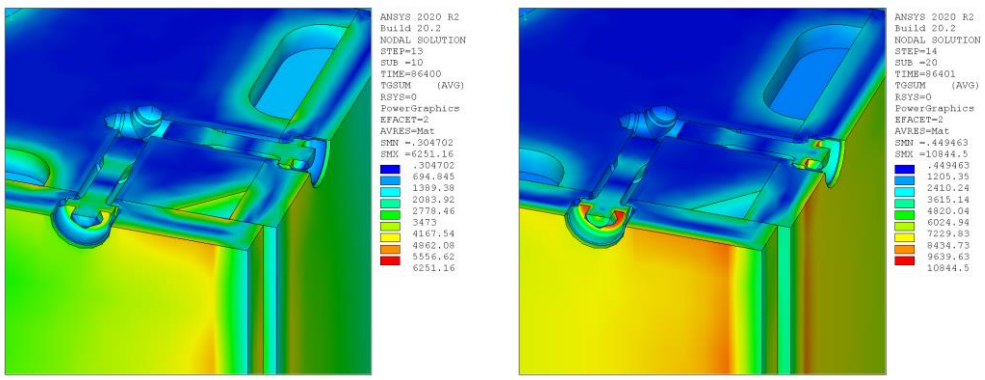

Figure 6. Thermal gradient [K/m]: nominal (Left) and SCRAM condition t+1s (Right)

STATIC STRUCTURAL ANALYSIS

The multi-step static structural analysis commences with the preloading of bolts, succeeded by the activation of the gravitational constant. Subsequent to these preliminary stages, a sequence of consecutive startup–nominal–SCRAM cycles is executed. Each cycle encompasses eight distinct steps, involving the application of a back pressure to the baffle plates (activation of pumps), imposition of the operational temperature distribution, application of neutron flux over a period analogues to a cycle (with a presumed capacity factor of 0.9), introduction of SCRAM temperature distributions (simultaneous with neutron flux removal), and the application of uniform room temperature. The cycle concludes with the removal of baffle plate back pressure (the shutdown of coolant pumps).

Normally, the analysis involves considering each cycle as a one-year duration, resulting in a total of 60 cycles spanning a total of 60 years. However, due to time constraints, the number of startup-nominal-SCRAM cycles was significantly reduced from 60 to 6. Consequently, to complete the analysis covering 60 years, the nominal operation step, resulting in dpa build-up was extended to 10 years each. Table 5 provides a summary of the load steps, delineating the initiation steps and first cycle.

Table 5: Static structural analysis, load steps

Load Step	Time	Applied loading
1	0.1	Preload bolts (9300 N for M12 and 18500 N for M16)
2	0.2	Lock bolts (Sliding contact -> bonded contact)
3	0.3	Activate gravity constant (9.81 m/s^2)
4	1	Apply hydraulic pressures as if coolant pumps are activated
5	2	Apply nominal operation temperature distribution
6	284018403	Apply (neutron) flux, resulting in dpa buildup
7	284018404	Apply SCRAM temperature distribution at t+0.5s
8	284018405	Apply SCRAM temperature distribution at t+1.0s
9	284018406	Apply SCRAM temperature distribution at t+10.0s
10	284018407	Apply uniform temperature distribution (22°C)
11	284018408	Remove hydraulic pressure as coolant pumps are shut down

Figure 7 shows the hydraulic pressure (load step 4), the nominal temperature distribution (load step 5), the dpa buildup after 60 years owing to the neutron flux (E > 1.0 MeV; max. 3.41 x 10^{13} n/cm²-s) during nominal operation (load step 6) and the temperature distribution at 1 second into SCRAM (load step 8).

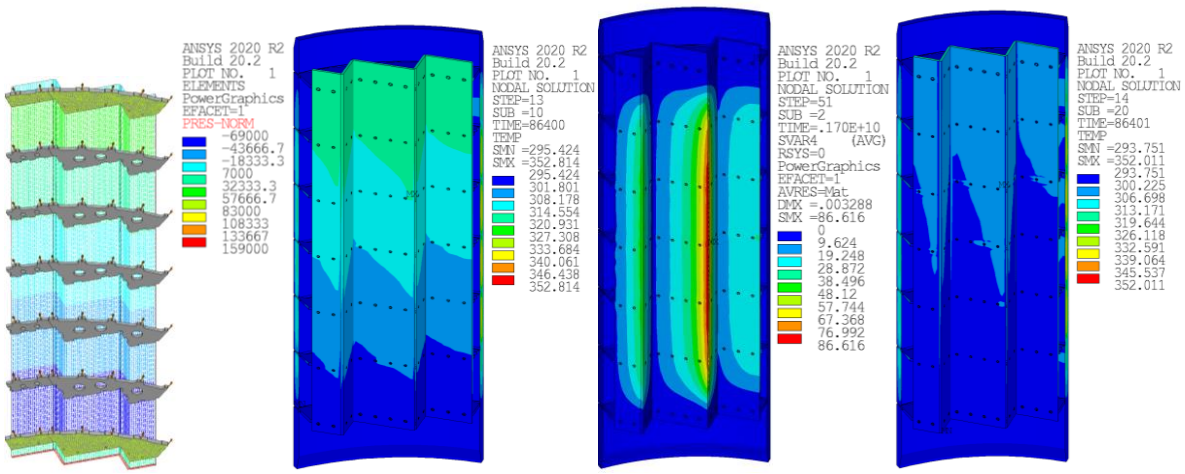

Figure 7. Baffle and former applied pressure [Pa] distribution (left), temperature distribution [°C] for nominal operation (mid) and SCRAM condition at t+1s (right).

SIMULATION RESULTS

Figure 8 shows the final swelling state after all simulation steps are completed. Both the results with the original as well as the modified creep coefficients is shown. It can be noted that the maximum swelling strain occurring with the original coefficients is significantly higher. The reason for this is that the implemented swelling function has a stress dependency component. Since stress relaxation occurs more readily with the modified creep coefficients, the swelling turns out less pronounced. Hence the lateral displacement of the baffle plate is reduced as well (from almost 3 mm to 2 mm).

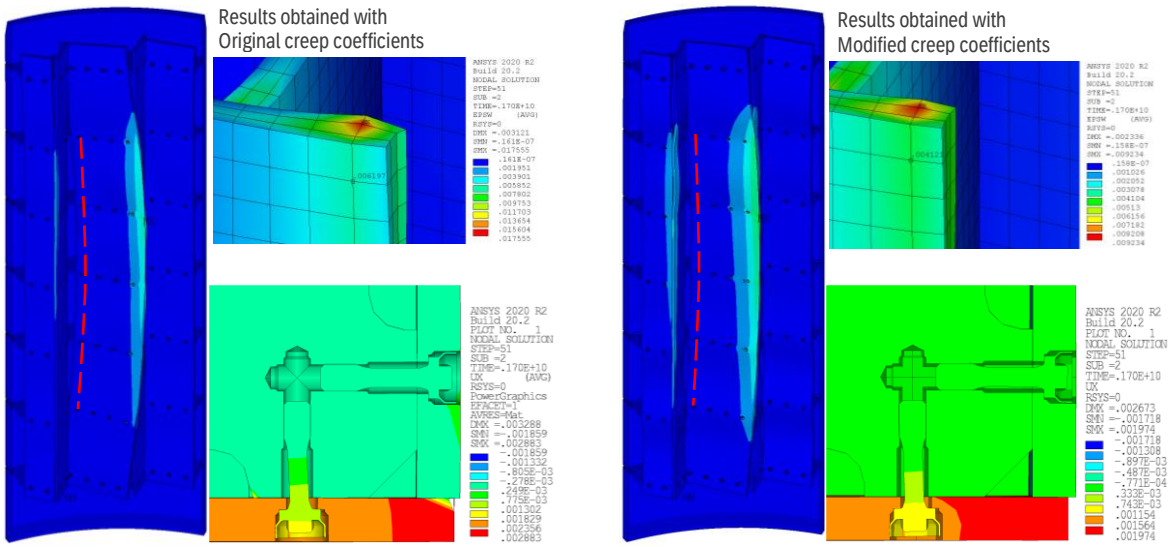

Figure 8. Swelling strain (scaled 30x) and baffle/bolt displacement [m] after 60 years (no scaling).

The effect of relaxation on absolute maximum bolt stress is significant. The effect is two-fold; it reduces the stress in the bolts directly, at the same time the reduced displacement of the baffle plates make for a less significant load exerted on the bolts.

Figure 9 show the peak stress that occurs over time for 5 different M12 baffle-former bolts present along the dotted red lines in Figure 8. The bolt at the center, where the largest lateral displacement occurs, exhibits the highest stresses over time.

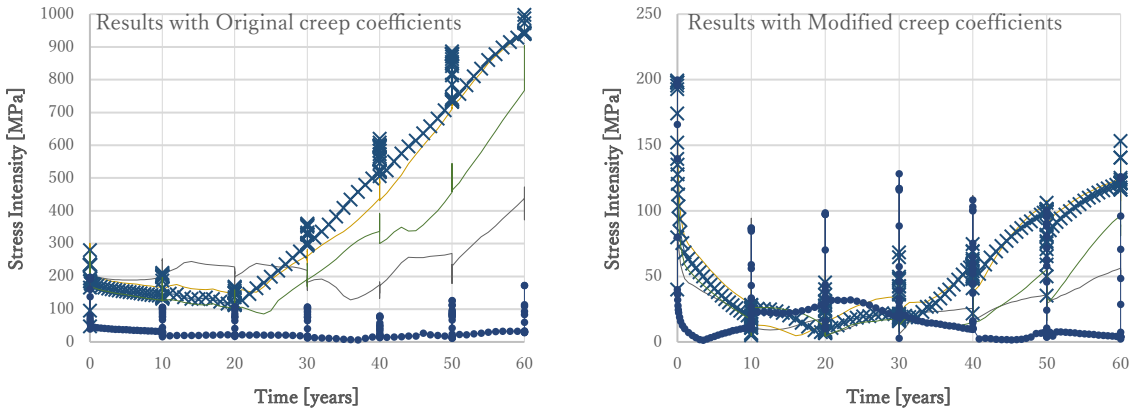

Figure 9. Stress evolution of M12 baffle-former bolts over time.

Figure 10 instead shows the peak stress that occurs over time for 7 different M12 barrel bolts present along a single column. The bolt at the top and bottom, exhibit the highest stresses over time. These bolts are fitted in the former plates that have the largest pressure differential applied over them.

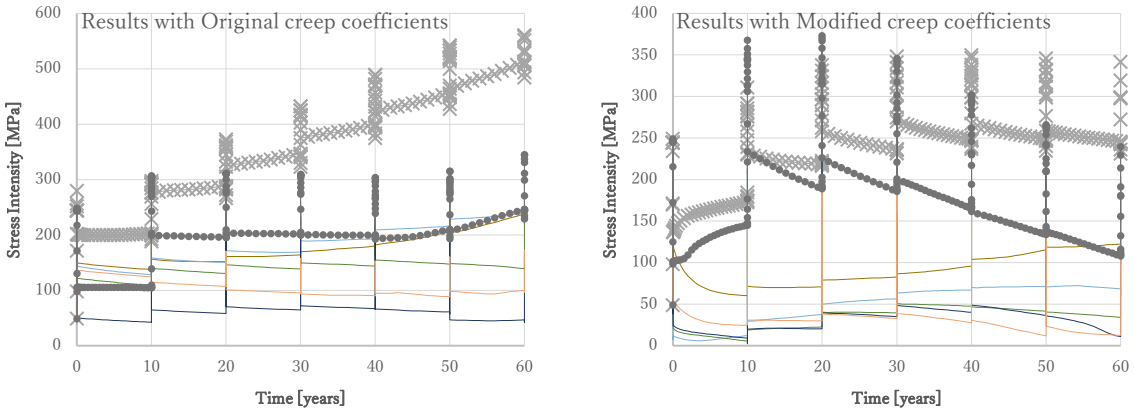

Figure 10. Stress evolution of M12 barrel bolts over time.

While the absolute stress reaches higher values in case of using the original creep coefficients, the stress range between the different load steps seem to imply a higher inclination towards fatigue damage in case of the modified creep coefficients. The larger stress range is the result of reduced preload on the bolts, resulting in a weaker overall structure, causing larger bending moments on the bolts due to vertical displacement of the baffle plates upon activation of the hydraulic pressure load.

The frictional interactions among various components may occasionally result in abrupt sub-step outcomes when friction is suddenly overcome, leading to the release of stored elastic energy. This phenomenon is particularly evident during the midpoint of neutron flux load steps, as depicted in the bolt stress graphs. To mitigate this issue, running the analysis for 60 cycles of 1 year each, rather than 6 cycles of 10 years each, should alleviate the problem as well as portray a more realistic scenario. This adjustment is expected to enhance predictability and facilitate a more controlled release of energy during each of the subsequent cool-down and/or hydraulic pressure removal load steps.

CONCLUDING REMARKS

Functionality of the RPV finite element model, incorporating constitutive irradiation and creep models, was demonstrated through a series of analysis, reflecting 60 year operational loads.

Modified creep coefficients demonstrated a reduction in swelling and displacement, resulting in lower secondary stresses. Stresses induced by hydraulic pressure however was increased, as the overall baffle-former-barrel structure was weakened due to relaxation of the bolts. This study advances our understanding of thermal, mechanical, and irradiation factors influencing the loads on the different bolts in the structure, stressing the importance of accurate modeling and foreseeing potential consequences of material property variations. Future work should refine models, validate against experimental data, and explore additional operational scenarios to enhance our understanding of mechanisms involved with SCC.

REFERENCES

Chopra, O. K. (2010). Degradation of LWR Core Internal Materials Due to Neutron (NUREG/CR-7027, ANL-10/11). U.S. Nuclear Regulatory Commission, Division of Engineering, Office of Nuclear Regulatory Research. Argonne National Laboratory.

DIN 17440 (1985). Nichtrostende Stähle; Technische Lieferbedingungen für Blech, Warmband, Walzdraht, gezogenen Draht, Stabstahl, Schmiedestücke und Halbzeug.

Matteoli, C., Hannink, M. H. C., et al. (2014). "Thermo-mechanical Analysis of PWR Bolts Susceptible to IASCC." Fontevraud 8 Conference, Avignon, September 2014.

Takakura, K., Sakima, K., et al. (2010). “In-pile Creep Behavior of Type 316 Stainless Steel at HALDEN Reactor.” *Proceedings of Fontevraud 7*, Avignon, France, O15-A132-T02.